Supporting Information

Mittag *et al.* 10.1073/pnas.0809222105

SI Materials and Methods

NMR Experiments: Assignments. Unphosphorylated and phosphorylated Sic1 1–90 wild-type (WT) and pSic1^{pT45} samples at 0.25–0.35 mM [in PBS (pH 7.0), 1 mM EDTA, 0.2% NaN_3] were used for assignment experiments. Triple-resonance assignment experiments (1) were performed at 800 MHz including CBCA(CO)NNH and HNCACB to examine C_α/C_β chemical shifts. *Cis*- and *trans*-prolyl isomers were assigned based on population ratios and C_β and C_γ chemical shifts obtained from CCC-TOCSY experiments. All spectra were referenced by using the internal reference DSS (sodium 2,2-dimethyl-2-silpentace-5-sulfonate). Data were processed by using NMRPipe (2) and analyzed by using NMRView (3). We used the program SSP (4) to combine C_α and C_β chemical shifts for different nuclei into a single secondary propensity (SSP) score representing the expected fraction of α-helical or extended structure at a given residue. The chemical shifts were weighted by their sensitivity to α- and β-structure. Chemical shifts of phosphorylated residues were ignored because of a lack of chemical shifts for comparison in the Biological Magnetic Resonance Bank (BMRB). The plots were smoothed by using weighted averaging over 5 residues.

Pulsed-Field Gradient (PFG) Diffusion Experiments. Experiments were carried out with 2.5 μL of 1% dioxane used as an internal standard with an effective hydrodynamic radius (R_h^{ref}) of 2.12 Å. Fitting of the signal intensities from protein or dioxane (i) as a function of gradient strength (g) to $i(g) = Ae^{-dg^2}$ allowed the extraction of the decay rates (d), which are proportional to the diffusion coefficients D. The protein hydrodynamic radius (R_h^{prot}) was calculated according to Eq. **S1** (5).

$$R_h^{prot} = \frac{d_{ref}}{d_{prot}}(R_h^{ref}) \qquad [S1]$$

Relaxation Experiments. ^{15}N R_1, $R_{1\rho}$, and heteronuclear NOE values were measured by using published pulse schemes (6) on 400 μM and 200 μM Sic1 and pSic1 samples, respectively, at 500 MHz. ^{15}N R_1 values were measured from 2D spectra recorded with the relaxation delays 10.1, 70.5, 151.1, 241.8, 342.6, 453.4, 594.5, and 755.7 ms. ^{15}N $R_{1\rho}$ values were measured from 2D spectra recorded with delays of 2, 12, 25, 41, 58, 78, 101, and 130 ms. ^{15}N R_2 values for each residue were calculated by correction of the observed relaxation rate $R_{1\rho}$ for the offset of the applied spin-lock RF field of 1,618 Hz to the resonance. Steady-state NOE values for free Sic1 and pSic1 were obtained with saturation of ^1H for 5-s and a 7-s delay between scans and without ^1H saturation by using a 12-s delay between scans. Steady-state NOE values of the complex were measured on a 100 μM pSic1 sample at a Skp1–Cdc4:pSic1 molar ratio of 1.2:1 with saturation of ^1H for 6 s. All datasets were processed by using NMRPipe (2).

Models of a polypeptide chain with unrestrained segmental motions predict R_2 relaxation rates that reach a plateau in the middle of the sequence whereas the protein termini exhibit smaller relaxation rates. The observation of regions of residues with higher relaxation rates indicates the presence of transient secondary or tertiary structure. The distribution of relaxation rates as a function of the sequence was fitted to

$$R(i) = R_{intrinsic}\sum_{j=1}^{N} e^{-\frac{|i-j|}{\lambda_0}} + \sum_{cluster} R_{cluster}e^{-\frac{|i-X_{cluster}|^2}{\lambda_{cluster}}} \qquad [S2]$$

a sum of the segmental motion of the main chain and additional deviations centered on clusters of residues (7). The relaxation data together with PRE data from additional cysteine mutants and additional structural restraints will be used in the characterization of disordered-state ensembles of pSic1 by using our software ENSEMBLE (8) to provide insight into the nature of contacts for residues with enhanced R_2 rates.

Transferred Cross-Saturation (TCS) Experiments. Because the saturation scheme is highly selective for the aliphatic proton region, the irradiation does not affect the intensity of the pSic1 amide region. However, to ensure that TCS effects seen for different phosphorylation sites are not transmitted by spin diffusion, a control experiment was carried out employing selective saturation of the T45 signal with a rectangular pulse with an RF amplitude of 17 Hz (see Fig. S5).

PRE Experiments. Site-directed mutagenesis was carried out by using the QuikChange PCR protocol (Stratagene) to build the Sic1 1–90 S38C mutant. The spin label was placed at residue Ser-38 to be close to 45 but far away enough not to disrupt the suspected tertiary interaction. The construct was verified by DNA sequencing. The mutant protein was expressed and purified analogously to the wild type, with the exception of the continuous presence of 5 mM DTT. After reversed-phase chromatography of the phosphorylated mutant and subsequent lyophilization, the protein was solubilized in PBS (pH 7.0), 5 mM DTT. DTT was removed by passing the protein through a PD-10 column (Amersham Pharmacia). The resulting protein solution was reacted with a 2-fold excess of MTSL label (Toronto Research Chemicals) and incubated overnight at 4 °C. Upon completion of the reaction, the protein solution was passed through a S75 gel filtration column to remove any unreacted label and to exchange into NMR buffer [PBS (pH 7.0), 1 mM EDTA, 0.02% NaN_3]. The yield of labeling was close to 100% as confirmed by mass spectrometry. The spin label was reduced by using a 5-fold excess of ascorbic acid to obtain the diamagnetic sample. Reduction efficiency was close to 100% as established by EPR. NH R_2 NMR experiments were performed at 500 MHz by using published pulse sequences (9) and analyzed by using NMRPipe (2). In the oxidized (paramagnetic) state, the unpaired electron of MTSL induces an enhanced relaxation of nearby nuclei whereas the reduced (diamagnetic) form serves as a reference state with no effects from the spin label. High PRE values thus indicate proximity of the spin label to the amide proton in question. The increase in PRE values around Tyr-14 is indicative of proximity to the spin label at residue 38, nearby to 45. This result supports the transient contact between Tyr-14 and Thr-45 derived from NMR relaxation and titration data. The very significant PRE effects throughout the chain are indicative of many tertiary interactions within pSic1, accounting for its high compactness.

1. Sattler M, Schleucher J, Griesinger C (1999) Heteronuclear multidimensional NMR experiments for the structure determination of proteins in solution employing pulsed-field gradients. *Prog Nucl Magn Reson Spectrosc* 34:93–158.
2. Delaglio F, *et al.* (1995) NMRPipe: A multidimensional spectral processing system based on unix pipes. *J Biomol NMR* 6:277–293.
3. Johnson BA, Blevins RA (1994) NMRView: A computer program for the visualization and analysis of NMR data. *J Biomol NMR* 4:603–614.

4. Marsh JA, Singh VK, Jia Z, Forman-Kay JD (2006) Sensitivity of secondary structural propensities to sequence differences between α- and γ-synuclein: Implications for fibrillation. *Protein Sci* 15:2795–2804.
5. Wilkins DK, *et al.* (1999) Hydrodynamic radii of native and denatured proteins measured by pulse-field gradient NMR techniques. *Biochemistry* 38:16424–16431.
6. Farrow NA, *et al.* (1994) Backbone dynamics of a free and a phosphopeptide-complexed Src homology 2 domain studied by ^{15}N NMR relaxation. *Biochemistry* 33:5984–6003.
7. Klein-Seetharaman J, *et al.* (2002) Long-range interactions within a nonnative protein. *Science* 295:1719–1722.
8. Marsh JA, *et al.* (2007) Improved structural characterizations of the drkN SH3 domain unfolded state suggest a compact ensemble with native-like and nonnative structure. *J Mol Biol* 367:1494–1510.
9. Donaldson LW, *et al.* (2001) Structural characterization of proteins with an attached ATCUN motif by paramagnetic relaxation enhancement NMR spectroscopy. *J Am Chem Soc* 123:9843–9847.
10. Borg M, *et al.* (2007) Polyelectrostatic interactions of disordered ligands suggest a physical basis for ultrasensitivity. *Proc Natl Acad Sci USA* 104:9650–9655.

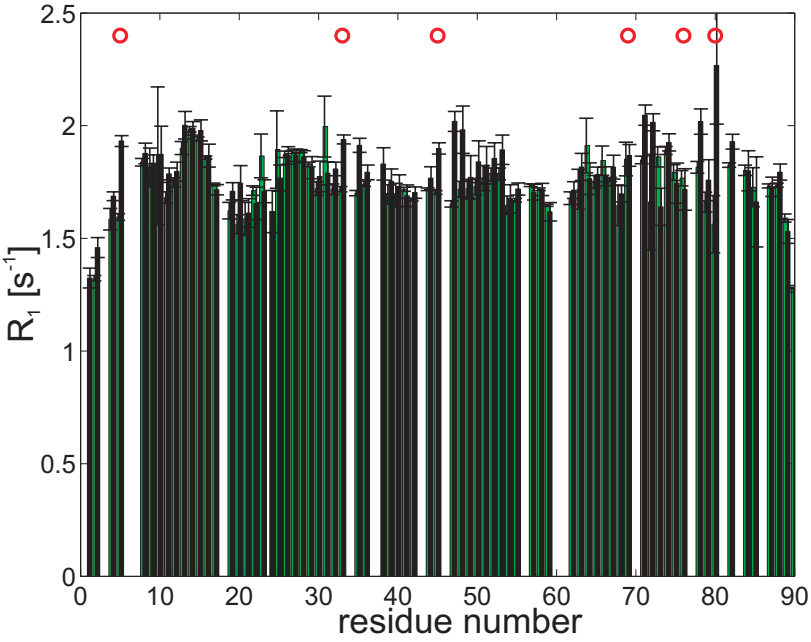

Fig. S1. Longitudinal ^{15}N relaxation rates of Sic1 (green bars) and pSic1 (black bars). Red circles indicate phosphorylation sites.

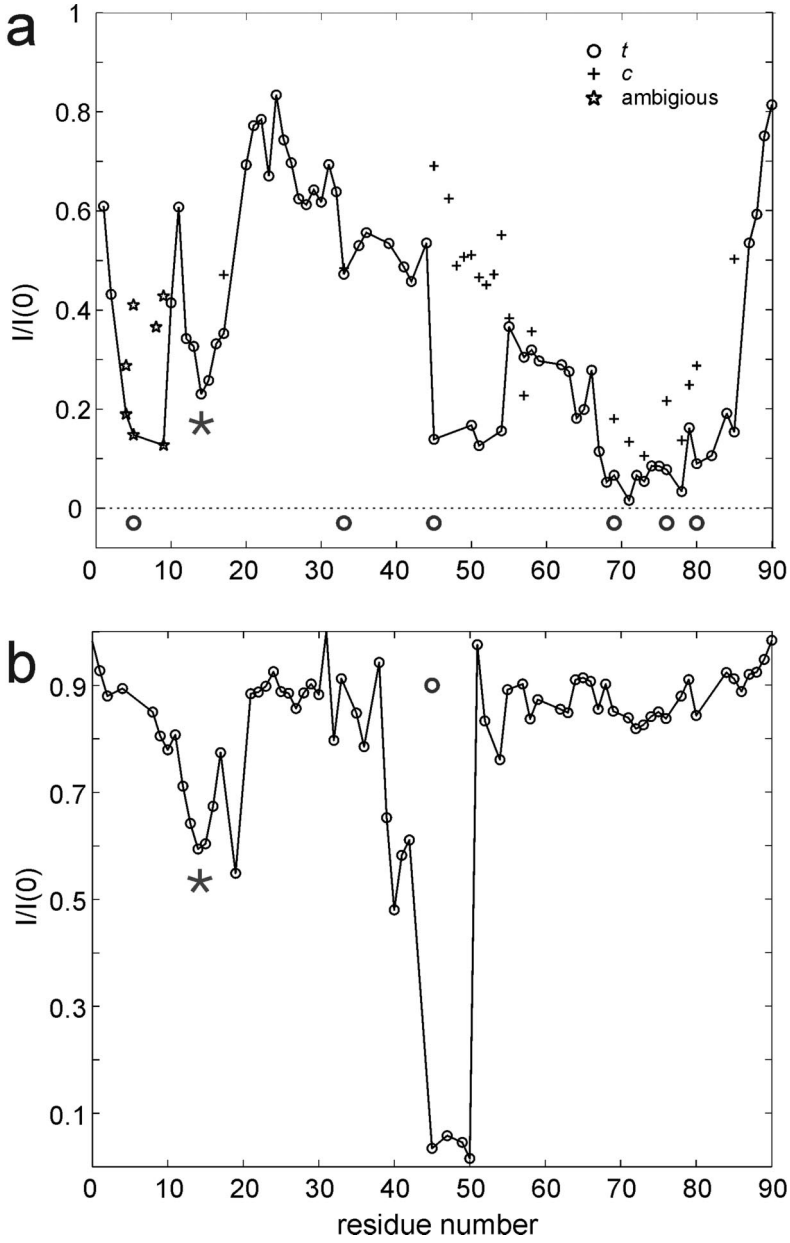

Fig. S2. Broadening of amide resonances of pSic1 in the presence of Skp1–Cdc4 reveals multiple binding sites undergoing only local ordering. (*a*) Intensity ratios of HN-N correlations for fully phosphorylated Sic1 (360 μM) upon titration with Skp1–Cdc4$^{263–744}$ [I(pSic1+ Skp1–Cdc4)/I_0] are plotted as a function of residue number for a Cdc4:pSic1 molar ratio of 0.75 for *trans*- (circles) and *cis*-prolyl isomers (crosses). In cases of >2 isomers, only effects for *cis*- and *trans*-isomers with respect to the $P+1$ proline of the CPDs are reported with the other prolines being in the *trans* conformation. Where only 1 symbol is plotted, *cis*- and *trans*-prolyl isomers were not resolved. Because isomers could not be assigned unambiguously in the region around pThr-5, effects for all isomers in this region are depicted as stars. However, lines are plotted through the most broadened isomers as a guide. Note that the interaction of pSer-80 with the secondary site of Cdc4 while pSer-76 is in the primary site explains the considerable broadening effect for the Pro-77 *trans*-, Pro-81 *cis*-isomer resonance of pSer-80 (cross). Phosphorylation sites are highlighted with red circles, and Tyr-14 is marked with a green asterisk. Note that broadening in the region around Tyr-14 is not localized to a CPD. We attribute it to a transient contact with one of the CPDs (see *b*), resulting in effective tumbling of Tyr-14 together with the large complex. (*b*) Intensity ratios of HN-N correlations for a Sic1$^{1–90}$ mutant phosphorylated only at position Thr-45 (pSic1^{pT45}, 230 μM) upon titration with Skp1–Cdc4$^{263–744}$; [I(pSic1^{pT45} + Skp1–Cdc4)/I_0] are plotted as a function of residue number for a Cdc4:pSic1^{pT45} molar ratio of 0.98 (circles). The position of pThr-45 is indicated by a red circle. Unlabeled Skp1–Cdc4 complex was titrated into a solution of labeled pSic1^{pT45}, and the ratios of NMR resonance intensities of pSic1^{pT45} in the free form and in the presence of Skp1–Cdc4 were plotted as a function of residue position. Approximately 8 residues around the Thr-45 phosphorylation site were broadened. This strong broadening dominating the pSic1^{pT45} data was effectively distributed among all weak CPD sites in the wild-type protein (*a*). This result demonstrates that a singly phosphorylated version of Sic1 can interact at least transiently with Cdc4 with primarily local ordering around the Thr-45 CPD motif and no global disorder-to-order transition. As in the titration of pSic1 with Skp1–Cdc4, an additional minimum was observed around Tyr-14 (*a* and *b*, green asterisk). The Tyr-14 site is at the center of a cluster of residues with restricted motion that is apparent in the ^{15}N relaxation data (Fig. 2*A*) of free pSic1. This suggests the presence of a tertiary contact between regions around Thr-45 and Tyr-14, which is also supported by hydrodynamic data (Table S3) and PRE data obtained for isolated pSic1 (Fig. S3). PRE data confirm the presence of many tertiary interactions along the pSic1 chain.

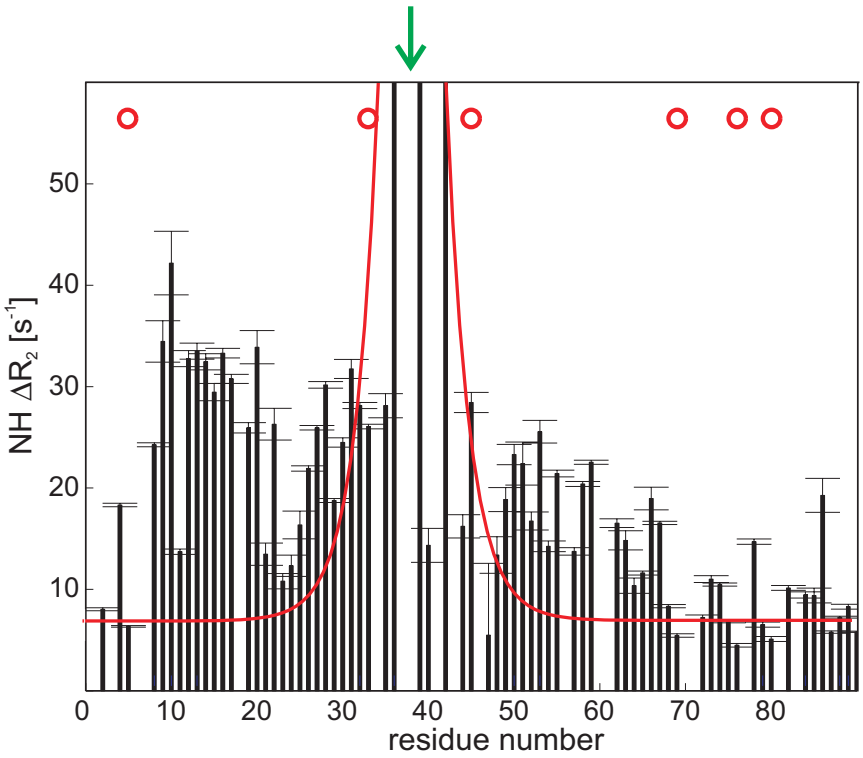

Fig. S3. PREs reveal transient contacts in spin-labeled pSic1 S38C. PRE values are calculated as the difference of NH R_2 rates of paramagnetic and diamagnetic pSic1 S38C and are plotted as a function of the residue number. The arrow indicates the position of the spin label MTSL [(1-oxyl-2,2,5,5-tetramethyl-3-pyrroline-3-methyl)-methanethiosulfonate]; red circles indicate the positions of phosphorylation sites. Red lines indicate the expected PRE profile in the case of a random coil model. Note that the very significant PRE effects throughout the chain are indicative of many tertiary interactions within pSic1, accounting for its high compactness.

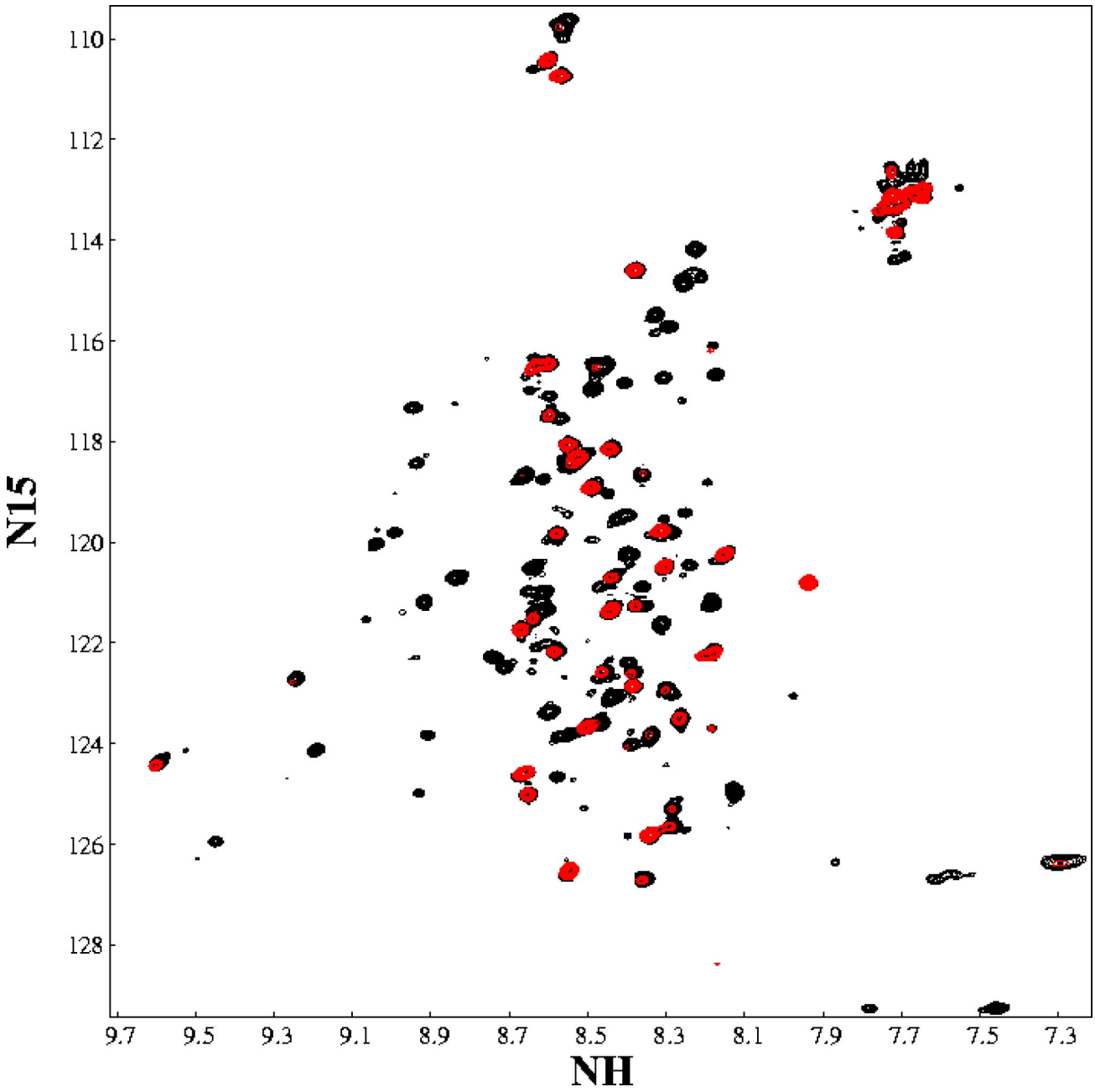

Fig. S4. $^{1}H^{N}$-^{15}N correlation spectra of free pSic1 and in complex with Skp1–Cdc4 demonstrates the disordered nature of large parts of pSic1 in the complex. ^{1}HN-^{15}N correlation spectra of free pSic1 (black) and in complex with Skp1–Cdc4 (red) at a molar ratio of Skp1–Cdc4:pSic1 of 1.2:1, at which 99% of pSic1 is bound, reveal broadening of many residues, particularly around the CPDs. However, the many observable and relatively sharp signals in the complex, having chemical shifts that are nearly unaltered, provide firm evidence that pSic1 remains significantly disordered.

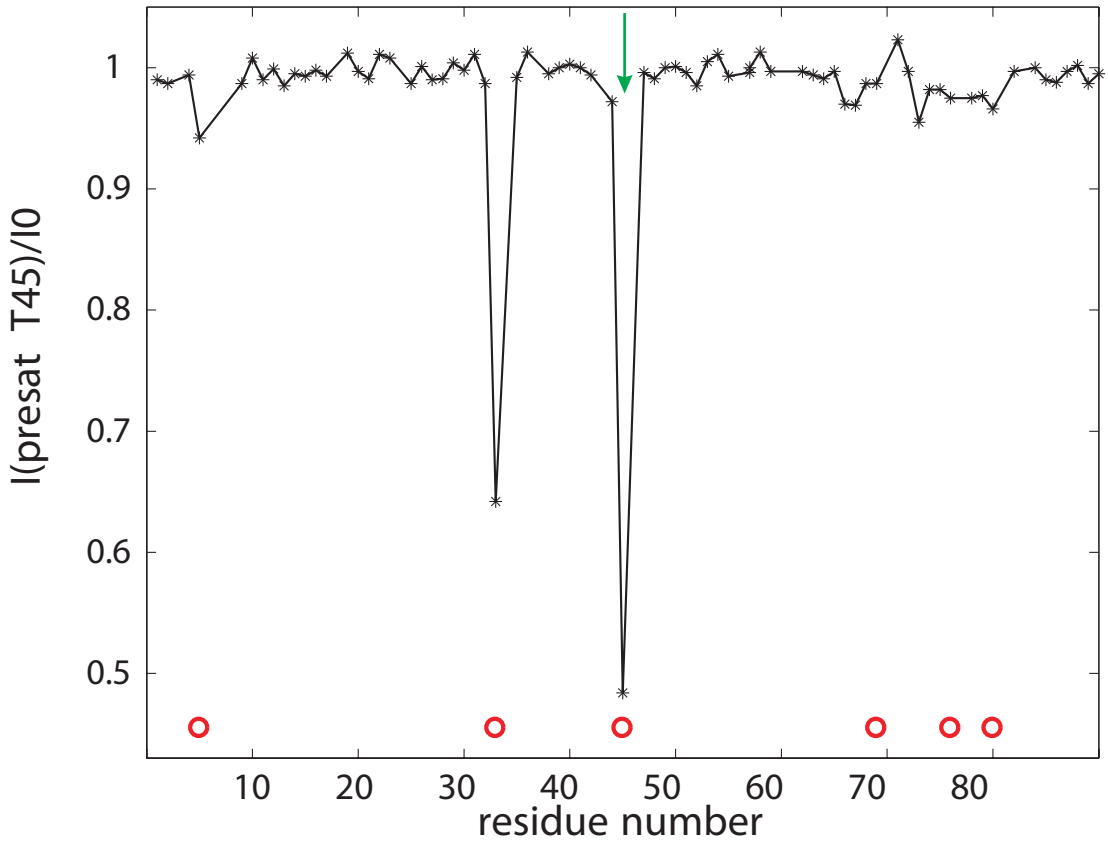

Fig. S5. TCS control experiment excludes spin diffusion between phosphorylation sites. A control experiment that used specific saturation of the resonance of interacting pT45 in a sample of ^{2}H, ^{15}N WT pSic1 (with 3.8 mol% Skp1–Cdc4$^{263–744}$ present) established that the observed TCS effects are caused by a direct interaction with Cdc4 but not by spin diffusion from an interacting phosphorylation site to a noninteracting one in the complex between pSic1 and Skp1–Cdc4. A selective radiofrequency (RF) pulse was used to presaturate the signal of pThr-45 (green arrow in plot), which therefore shows considerably reduced intensity. The closest signal (pThr-33) has a frequency separation of only 83 Hz. The reduced intensity observed for pThr-33 is thus caused by partial saturation from the RF pulse instead of by spin diffusion. Intensity ratios close to unity for other signals establish that the TCS effects (Fig. 3*A*) are not caused by spin diffusion. The ratio of intensities of signals with and without presaturation were plotted. Phosphorylation sites are highlighted with red circles.

Table S1. Cdc4 phosphodegrons (CPDs) in Sic1

Sic1 (9 suboptimal CPD sites)	
T2	Nt-M-pT-P-S-T-P-P
T5	P-S-pT-P-P-R-S-R
T33	Q-K-pT-P-Q-K-P-S
T45	P-V-pT-P-S-T-T-K
S69	M-T-pS-P-F-N-G-L
S76	L-T-pS-P-Q-R-S-P
S80	Q-R-pS-P-F-P-K-S
T173	P-G-pT-P-S-D-K-V
S191	N-N-pS-P-K-N-D-A

Cdc4 phosphodegron (CPD) consensus L/I-L/I/P-pT-P-<RK>$_4$, where <...> indicates that these residues are disfavored.

Table S2. Affinities of Sic1 phosphopeptides for Cdc4 from intrinsic Trp fluorescence-binding experiments

Peptide name	Peptide sequence	K_d, μM	Net charge	Net charge Sic1*
Affinity of 6-fold phosphorylated Sic1 1–90				
pSic1		~0.6	−1	
Affinities of peptides representing different Sic1 phosphorylation site regions†				
$Sic1^{10pT2/pT5}$	Ac-MpTPSpTPPRSR-NH_2	14.2 ± 4.1	−2	7
$Sic1^{9pT33}$	Ac-GQKpTPQKPS-NH_2	~145	0	9
$Sic1^{9pT45}$	Ac-VPVpTPSTTK-NH_2	72.2 ± 1.8	−1	9
$Sic1^{20pS69/pS76/pS80}$	Ac-GMTSPFNGLTpSPQRpSPFPKS-NH_2	2.4 ± 0.2	−4	5

Results are the average of at least three individual fluorescence-binding experiments with SE of all measurements reported. Values for which only one experiment reached saturation of binding are indicate as approximate (~).

*Net charge of Sic1 1–90 with the same residues phosphorylated as the peptide.

†Short phosphopeptide data reported in ref. 10.

Table S3. Sic1$^{1-90}$ sequence

```
MTPSTPPRSR GTRYLAQPSG NTSSSALMQG QKTPQKPSQN LVPVTPSTTK
 2  5         14                   33           45
SFKNAPLLAP PNSNMGMTSP FNGLTSPQRS PFPKSSVKRT
                   69      76  80
```

CDK phosphorylation sites are bold, prolines are italic.

Table S4. Hydrodynamic radii of Sic1 1–90 from NMR PFG experiments

Protein	Temperature,°C	R_h, Å	Error*, Å
Sic1 (nonphospho)	5	21.5	1.1
pSic1	5	19.7	0.9
pSic1	10	20.2	0.9
pSic1	15	18.0	0.9
pSic1	20	19.4	1.6
pSic1	25	19.3	1.4
pSic1 Y14A	5	23.5	2.2
pSic1 Y14A	25	23.2	0.5
pSic1 T45A	25	23.1	0.3
90-residue denatured		28.7†	
90-residue globular		17.5†	

*Errors are calculated from uncertainties of decay rates by error propagation.
†Values are calculated according to equations in ref. 5.